The Preparation of CuO@ZnO Core-Shell Materials as High-Stability Anodes for Lithium-Ion Batteries

Bo Liu[1], Yongming Chuan[1], Yinyin Zhang[1], Jiajiao A[1], Haiyun Chen [1,], Tasawar Hayat[2], Ahmed Alsaedi[2] and Bashir Ahmad[2]*

[1] School of Chemistry and Environment, Yunnan Minzu University, Kunming 650500, China
[2] Department of Mathematics, King Abdulaziz University, Jeddah 21589, Saudi Arabia.
[*]E-mail: chenhy1960@163.com

In this study, CuO@ZnO core-shell composite materials were successfully reported by chemical processes of depositing ZnO on the CuO surface. When evaluated as a lithium-ion battery anode, the CuO@ZnO composite shows a higher specific capacity of 300 mAh g^{-1} at 0.2 C after 100 cycles, especially CuO@ZnO-6.5% (the molar ratio of CuO to ZnSO$_4$·7H$_2$O of 1:0.065) composite material electrode still holds 459.5 mAh g^{-1} discharge capacity after 500 cycles. The test results show that the excellent coating on the CuO@ZnO composites improves the stability performance as electrodes for lithium-ion batteries due to the mechanism of ZnO. Therefore, the certain coverage of the CuO@ZnO composite electrode results in a valuable material for anodes in future batteries.

Keywords: Lithium-ion battery, Anode material, CuO@ZnO composites

1. INTRODUCTION

Advanced electrode material is the centre of the future energy storage device [1-3]. Transition metals oxides (TMOs) have a high theoretical specific capacity for use as an alternative anode material for lithium-ion batteries (LIBs) [4-9]. Among transition metal oxides, CuO is a good material for energy applications due to its high theoretical capacity, good chemical stability, non-toxicity, environmental benignity and abundant raw materials [10, 11]. However, the volume expansion, large irreversibility and rate limitations in the first cycle limited its development in engineering. To overcome these drawbacks, CuO performance can be improved by controlling the morphology [12], micro/nanostructure design [13], and composite preparation [14].

Yin et al. prepared hollow porous CuO@C composite microcubes, and it achieved a highly reversible capacity (510.5 mAh g-1 after 200 cycles) [15]. Wang et al. prepared CuO@Ag composite materials that improved the electronic conductivity of the electrode, which exhibited excellent cycling

performance [16]. Yin et al. synthesized a polypyrrole (PPy)-coated CuO nanocomposite, and the material shown a high reversible capacity, reached760 mAh g^{-1} [17]. Qing et al. prepared a CuO@MnO$_2$ core-shell material, and the core-shell architecture through reinforcement or modification resulted in enhanced electrochemical propertie^s [18]. Therefore, a core-shell structure can be prepared to enhance the electrochemical performance of CuO.

The work mainly improves the performance of CuO by preparing a core-shell structure. The core-shell structure can maintain electrolyte penetration, reduce agglomeration during Li$^+$ intercalation, and improve the electrochemical performance [17]. According to research, the mechanism of ZnO with Li not only contains alloying/dealloying process and also ZnO reduction/oxidation process, which is same with 3d transition metal oxides [19].

Herein, CuO@ZnO core-shell composites were successfully prepared. ZnO as an ideal candidate material due to its high theoretical capacity of 978 mAh g^{-1}, higher lithium-ion diffusion coefficient compared to that of other transition metal oxides, and cost benefit [20]. When used as the LIB anode, the CuO@ZnO composites showed high capacity and good cycling stability. Note that the CuO@ZnO-6.5% composite exhibited the highest specific capacity of 459.5 mAh g^{-1} at 0.2 C after 500 cycles, which is higher than that of pure CuO.

2. EXPERIMENTAL

2.1 Preparation and characterization of the CuO@ZnO material

The CuO material was prepared based on the typical procedure in the literature [21]. The preparation process for the ZnO-coated CuO core-shell material was as follows. First, a certain amount of ZnSO$_4$·7H$_2$O (0.01 mol/L) aqueous solution (375 µL, 1125 µL, 1875 µL, 2347.5 µL, and 3000 µL), CO(NH$_2$)$_2$ (0.1 mol/L), and 10 mL deionized water were added to a round-bottom flask. The molar ratio of CO(NH$_2$)$_2$ to ZnSO$_4$·7H$_2$O was 8:1. Subsequently, the solution was mixed for 5 min, and then 0.3 g CuO was added. After stirring for 3 h under reflux, the product was collected and washed with deionized water, harvested centrifugation and redispersion cycles and dried at 60°C for 12 h. Finally, the dried sample was ground and calcined under an air atmosphere at 500°C for 3 h in a muffle furnace. The resulting CuO@ZnO core-shell material was obtained. According to the ZnSO$_4$·7H$_2$O content, we named the obtained CuO@ZnO core-shell material CuO@ZnO-n%, in which n denotes the concentration of ZnSO$_4$·7H$_2$O.

The morphologies of the CuO and CuO@ZnO composites were studied by field emission scanning electron microscopy (FESEM, FEI Nova Nano SEM 450). The crystal structure information of the composites was determined with XRD (BrukerD8 ADVANCE), which was recorded on a Cu target in the 2θ range from 20° to 80°. X-ray photoelectron spectroscopy (XPS) were conducted on a Ulvac-PHI, using Al Kα X-rays to analyse the valence state of the as-prepared samples. The binding energy obtained in the XPS analysis was calibrated against the C 1s peak at 284.8 eV.

2.2 Electrochemical tests of the CuO@ZnO material

CR2025 coin-type cells was used for testing the electrochemical performance. The working electrodes contained 80 wt.% active material, 20% acetylene black, SBR and CMC,, which were dissolved in water to form a slurry. A lithium sheet was used as reference electrode, and a Celgard 2320 membrane was used as the separator. The assembly of the coin cells was accomplished in an argon-filled glove box with O_2 and H_2O levels maintained at less than 1 ppm. Galvanostatic charge–discharge experiments were performed using the Land electric test system CT2001A at a current density of 0.2 C between 0.01 and 3.00 V. Cyclic voltammetry (CV) and Electrochemical impedance spectroscopy (EIS) measurements were performed on an electrochemical workstation (CHI604D, Chenhua).

3. RESULTS AND DISCUSSION

3.1 Structure and morphology
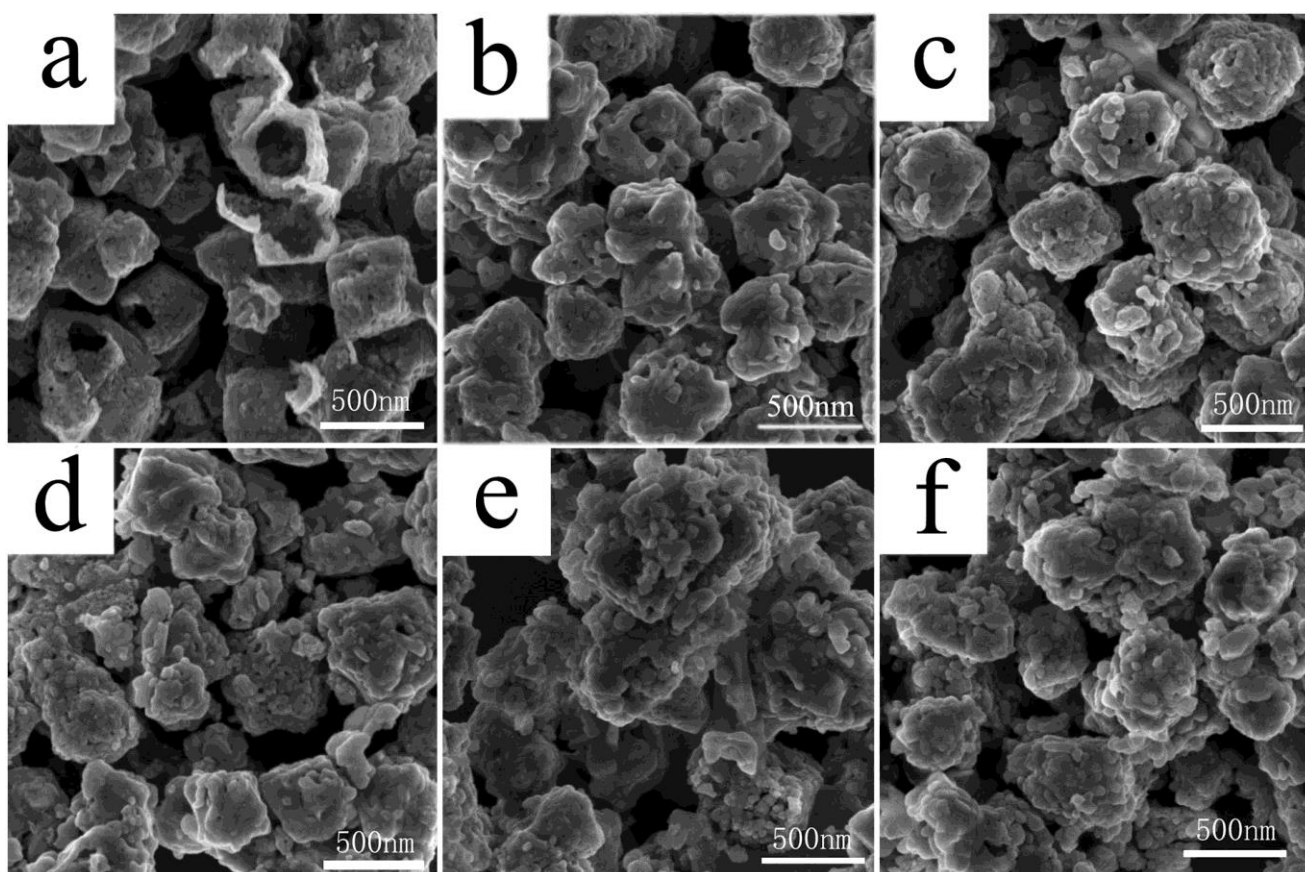
Figure 1. SEM images of (a) CuO, (b) to (f), are 1%, 3%, 5%, 6.5% and 8% coated CuO@ZnO composites.

SEM images of CuO and the CuO@ZnO composites are displayed in Fig. 1. The CuO sample has a uniform hollow octahedral morphology approximately 400 nm in diameter. The evolution of the morphology of the CuO@ZnO composites is shown in Fig. 1b–f. Before the coating, the CuO surface is rough with some pores, and part of the CuO octahedral morphology is broken, but after the coating, the surface of the material becomes denser and smoother (Fig. 1b). As shown in Fig. 1c, there are some pores and some other irregular morphologies in the material that is deposited on the surface of CuO. Fig. 1d-f indicates that with increasing Zn content, the deposition on the surface of the material increases. In this context, we can judge that CuO is coated with ZnO. There are a large number of particles with an irregular morphology and rod-like structures on the CuO surface, which increase the specific surface area of the material and the contact surface of the electrolyte and electrode materials. Furthermore, because ZnO has an excellent lithium-ion diffusion ability compared to that of transition metal oxides [22] and bare CuO has poor ion transport kinetics [23], the composites greatly improved the lithium-ion diffusion ability of bare CuO.

Table 1. EDX data for pure CuO and CuO@ZnO composites.

Element	CuO At%	CuO@ZnO -1%At%	CuO@ZnO -3%At%	CuO@ZnO -5%At%	CuO@ZnO -6.5%At%	CuO@ZnO -8%At%
C	-----	5.49	5.51	5 .38	5.25	5.01
O	44.88	32.88	41. 93	42.09	42.65	40.41
Cu	51.00	60.49	50.27	49.59	48.96	50.24
Zn	-----	1.14	2.29	2.94	3.14	4.34

The EDX analysis results of the element distribution in the CuO@ZnO composites are presented in table 1. Cu and O from the CuO material can be seen. When CuO is coated with ZnO, the signals of Cu, O, C and Zn can be detected. With increasing ZnO usage, the content of Zn also increased. The percentages of Zn are 1.14%, 2.29%, 2.94%, 3.14% and 4.34%. By calculation, the ZnO contents are 1.9%, 4.6%, 5.9%, 6.4% and 8.6%, respectively. In this context, all five coating materials have ZnO. Finally, it can be found that the content of ZnO detected by EDX corresponds with the usage in the experience. Moreover, it is obvious that with increasing content, the proportion of Zn increases, which is consistent with the SEM results.
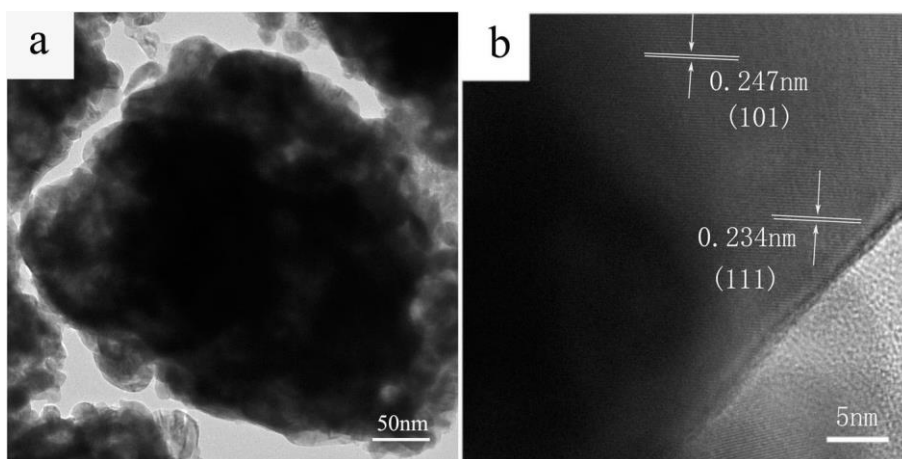
Figure 2. TEM images (a) and HRTEM images (b) of the CuO@ZnO-6.5% sample.

To further understand the microscopic structure of the CuO@ZnO composites, they are shown in Fig. 2. The TEM image of the CuO@ZnO-6.5% sample is shown in Fig. 2(a). To examine the ZnO in the sample, high-resolution lattice fringe tests on the sample were carried out and are shown in Fig. 2(b). The result shows that the obvious lattice spacing of 0.234 nm could be indexed to the (111) crystal plane of CuO. Moreover, the lattice fringes with a spacing of 0.247 nm correspond to the (101) planes of the ZnO crystal [24]. TEM tests verified that ZnO was successfully coated on the surface of CuO.
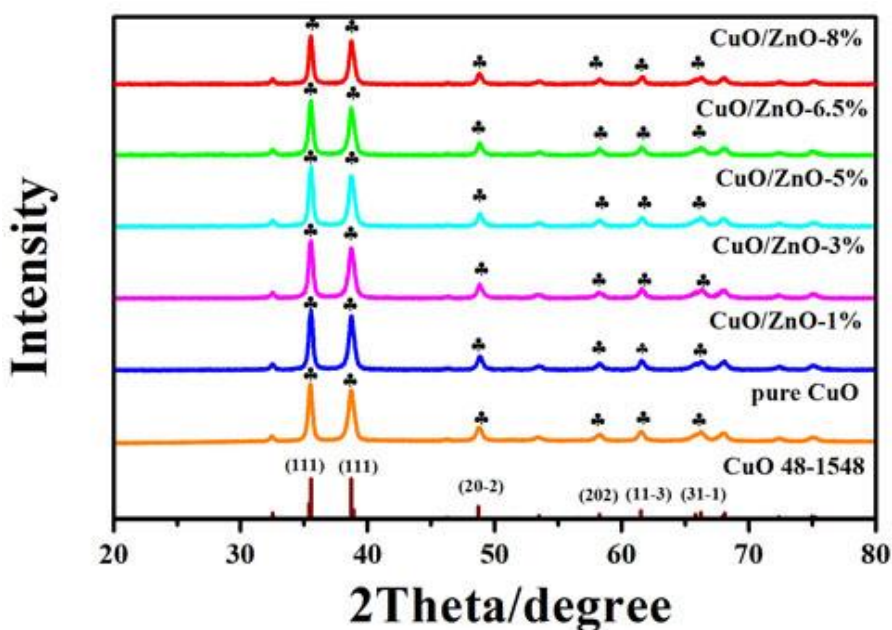
Figure 3. XRD patterns of pure CuO and the CuO@ZnO composites.
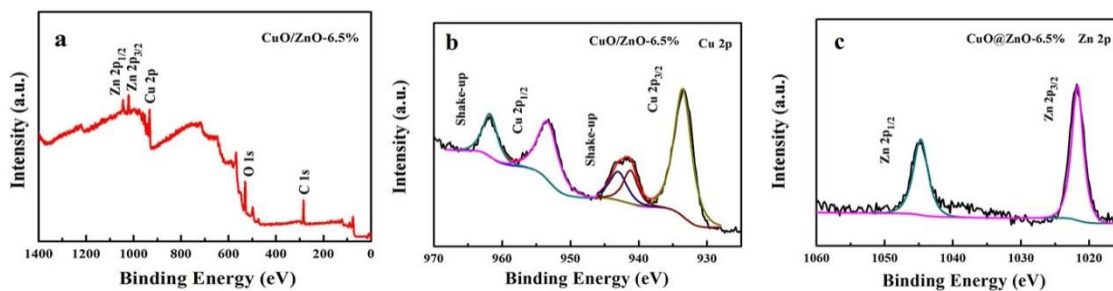
Figure 4. XPS survey spectra of the CuO@ZnO-6.5% sample (a). High-resolution Cu 2p spectra of CuO@ZnO-6.5% sample (b) and High-resolution Zn 2p spectra of CuO@ZnO-6.5% sample (c).

The structures of CuO and the CuO@ZnO composites with different coating amounts were examined by XRD, as shown in Fig. 3. As can be seen, the six samples have similar crystallographic structures. Clearly diffraction peaks appeared at $2\theta= 35.5°, 38.7°, 48.7°, 58.2°, 61.5°$ and $66.2°$ and can be assigned to the (1 1 -1), (1 1 1), (2 0 -2), (2 0 2), (1 1 -3) and (3 1 -1) crystal planes, respectively, of CuO based on the PDF file No. 48-1548. In addition, the CuO@ZnO composites do not have the ZnO peak due to their low content. The detection limit of XRD is closely related to the dispersion of the substance to be detected and the type of substance. Different phases have different absorption of X-rays. However, the results show that CuO has well crystallinity, and the ZnO coated on the surface of CuO did not mask its crystallinity.

X-ray photoelectron spectroscopy (XPS) was performed on the CuO@ZnO composites. The XPS survey spectra of the CuO@ZnO-6.5% sample is shown in Fig. 4(a). High-resolution spectra of Cu 2p (Fig. 4(b)) show two main peaks at approximately 933.9 eV and 953.1 eV matching the binding energies of Cu $2p_{3/2}$ and Cu $2p_{1/2,}$ respectively, with a spin orbit splitting separation of 20 eV, which is consistent with the literature [25]. These peaks are typically attributed to Cu(II) states. The shake-up satellite peaks were placed at 941.5 eV and 943.1 eV, which correspond to the characteristic peaks of CuO, confirming the existence of the Cu(II) phase. The peaks of Zn $2p_{3/2}$ and Zn $2p_{1/2}$ are mainly located at 1021.7 eV and 1044.7 eV (Fig. 4(c)), respectively, which confirmed the existence of zinc in the Zn^{2+} form [26].By calculation, the content of ZnO is 58.7% in the CuO@ZnO-6.5% sample. By comparing XPS and EDX results, the ZnO content according to XPS is much higher than that of EDX, and this difference can prove that the CuO@ZnO composite is a core-shell material.

3.2. Electrochemical performance

The electrochemical performances of pure CuO and all the CuO@ZnO composites were investigated. Fig. 5(a) presents the cyclic performance of the anodes constructed from the pure CuO sample and the CuO@ZnO samples. For clarity, the pure CuO sample and the CuO@ZnO-6.5% sample charge-discharge performances are shown in Fig. 5(b) and 5(c). It is clearly shown that the capacity decays severely in the first cycle.
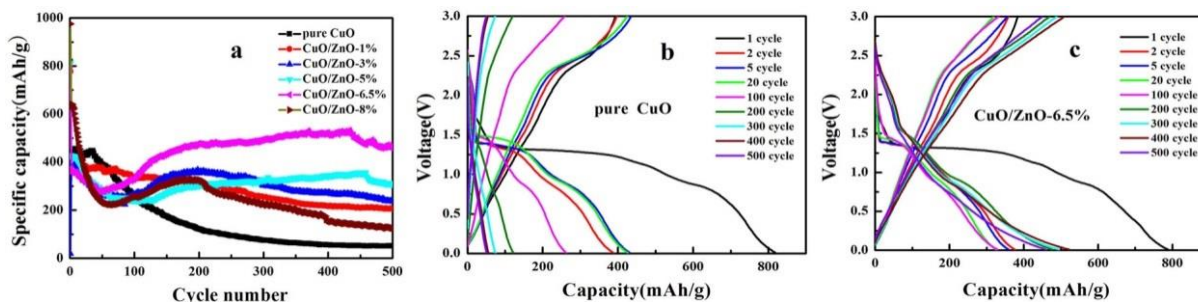
Figure 5. The cycle performance curves for all samples (a) and charge–discharge curves for selected cycles for the pure CuO sample (b) and 6.5% CuO@ZnO composite (c) in the potential range of 0.01–3.00 V at 0.2 C.

The irreversible capacity loss in the first cycle is a common phenomenon result by the formation of the SEI film and the irreversible phase transformation [27]. The CuO sample and CuO@ZnO-6.5% sample both have a high initial discharge specific capacity of approximately 700-900 mAh g^{-1}, while the theoretical discharge specific capacity only is 670 mAh g^{-1}. In addition, the specific capacity of the pure CuO sample gradually decreased in the 500 cycles, and the CuO@ZnO-6.5% sample specific capacity was concentrated at approximately 400 mAh g^{-1} in the 500 cycles. Similarly, as shown in Fig. 5(a), the capacity of the pure CuO electrode decays after 50 cycles, which is attributed to the pulverization of CuO during the charge-discharge processes [28]. In contrast, the charge-discharge curves of all CuO@ZnO samples were higher than those of the pure CuO sample after 130 cycles. After 100 cycles, the discharge specific capacity of the pure CuO sample decreased to below 200 mAh g^{-1}. By comparison, the discharge specific capacity of the CuO@ZnO-1% sample was approximately 300 mAh g^{-1} from the cyclic performance curves. The capacity trend first decreases and then increases for the CuO@ZnO samples coated with 3%, 5%, 6.5% and 8%. As the amount of ZnO increased, the cycling stability of the CuO@ZnO composites gradually increased. However, when the amount of ZnO was higher, the discharge capacity was not better.

CuO@ZnO-8% exhibits worse discharge-specific capacity than CuO@ZnO-6.5% material. In all, the CuO@ZnO-6.5% sample showed the best cycling stability among the six samples. The obtained results demonstrate that the lithium storage performance of the CuO@ZnO samples was greatly improved, which can be attributed to the core-shell structure. Such as Chen at al. had reported CuO@TiO$_2$ core-shell anode was prepared, it had excellent cyclic stability compared to the CuO anode [29]. Yang et al. had. prepared TiO$_2$@α-Fe$_2$O$_3$ core-shell nanostructures anode, it improved electrochemical performance than the TiO$_2$ anode [30]. As summarized in table 2. these core-shell structure materials can enhance the electrochemical performance and electrochemical stability of the pure materials. ZnO has excellent lithium-ion diffusion ability, and the drawback is from the large volume expansion (approximately 150%) and theinherent poor electronic conductivity.. For this, they are also limit its application [31, 32]. Therefore, a certain amount of ZnO provides an effective way to mitigate the capacity fading of a transition metal oxide material such as CuO as an anode material for LIBs.
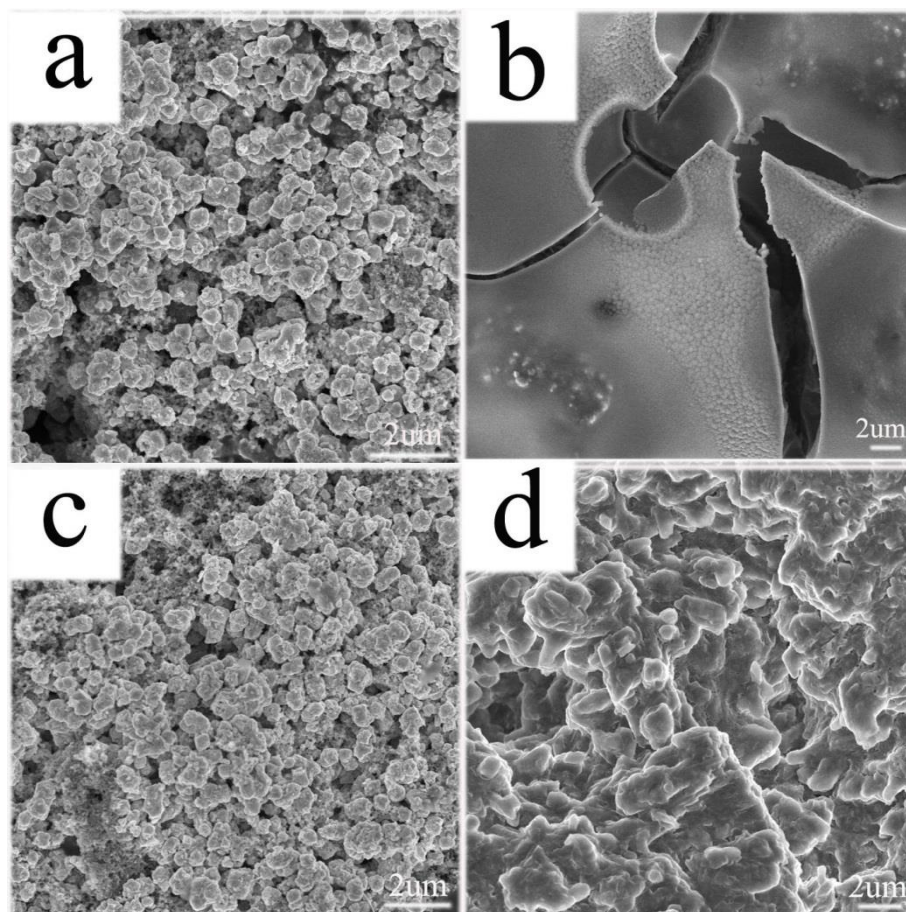
Figure 6. SEM images of CuO electrodes (a) fresh and (b) cycled 500 charge/discharge cycles. CuO@ZnO-6.5% electrodes (c) fresh and (d) cycled 500 charge/discharge cycles.

Table 2. List of the reported works on core-shell materials as anodes for lithium ion batteries

Marerials	Capacity	Cycles	Ref.
CuO	50mA h g^{-1}	500cycles	This work
CuO@ZnO-6.5%	500mA h g^{-1}	500cycles	This work
CuO	25mA h g^{-1}	100cycles	29
CuO@TiO$_2$	220mA h g^{-1}	100cycles	29
TiO$_2$	100mA h g^{-1}	500cycles	30
TiO$_2$@α-Fe$_2$O$_3$	800mA h g^{-1}	500cycles	30

Fig. 6 shows SEM images of fresh and cycled CuO electrodes and CuO@ZnO-6.5% electrodes. Fig. 6 shows that the CuO electrode morphology changed upon cycling. The CuO appeared the cracks after 500 cycles, while the composite electrodes did not exhibit obvious cracks, negatively affecting the battery performance. This result is corresponding to the fast capacity fading observed during 500 cycles with CuO.
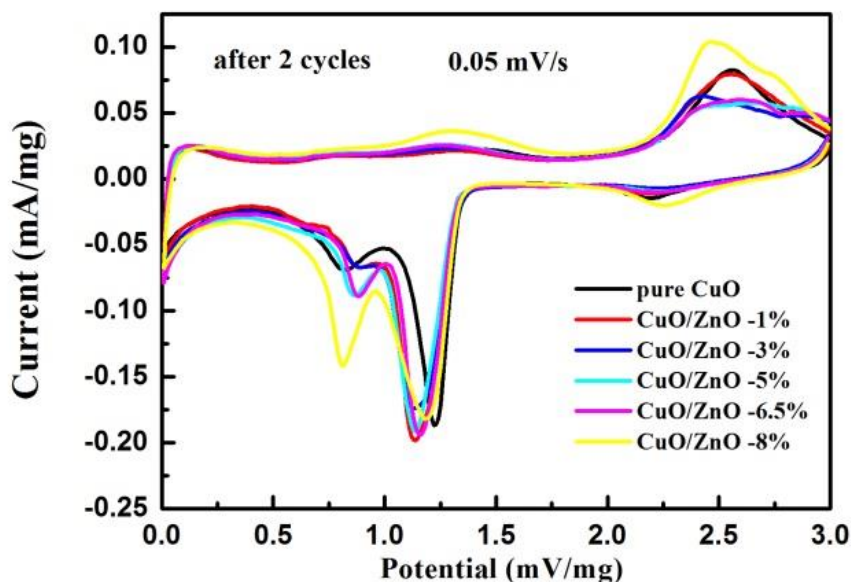
Figure 7. Cyclic voltammogram curves of pure CuO and the CuO@ZnO composites with different coating amounts after the second charge–discharge cycle in 0.01–3.00 V.

The cyclic voltammogram curves as shown in Fig. 7. The shapes of the CV curves for these samples are similar. One oxidation peak and two obvious reduction peaks are obvious. For pure CuO and CuO@ZnO composites with different coating amounts, the two reduction peaks are at 1.27 V and 0.89 V, which corresponds well with the discharge plateaus in Fig. 5. This similarity proved that the addition of ZnO does not change the lithiation-delithiation mechanism of CuO as an anode for lithium-ion batteries. The two reduction peaks correspond well with the discharge plateaus in Fig. 5(a). The reactions of Li with CuO are as follows:

$$2CuO + 2Li = Cu_2O + Li_2O$$
$$Cu_2O + 2Li = 2Cu + Li_2O$$
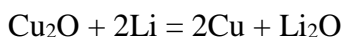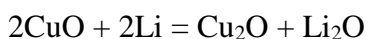
According to a previous study [33], the electrochemical reaction of Zn with lithium includes the reduction of ZnO into Zn and the formation of lithium-zinc alloy, which can be expressed as follow.

$$ZnO + 2Li \rightarrow Zn + Li_2O$$

$$Zn + Li \rightarrow LiZn$$

$$LiZn \longleftrightarrow Zn + Li$$

$$Zn + Li_2O \longleftrightarrow ZnO + 2Li$$
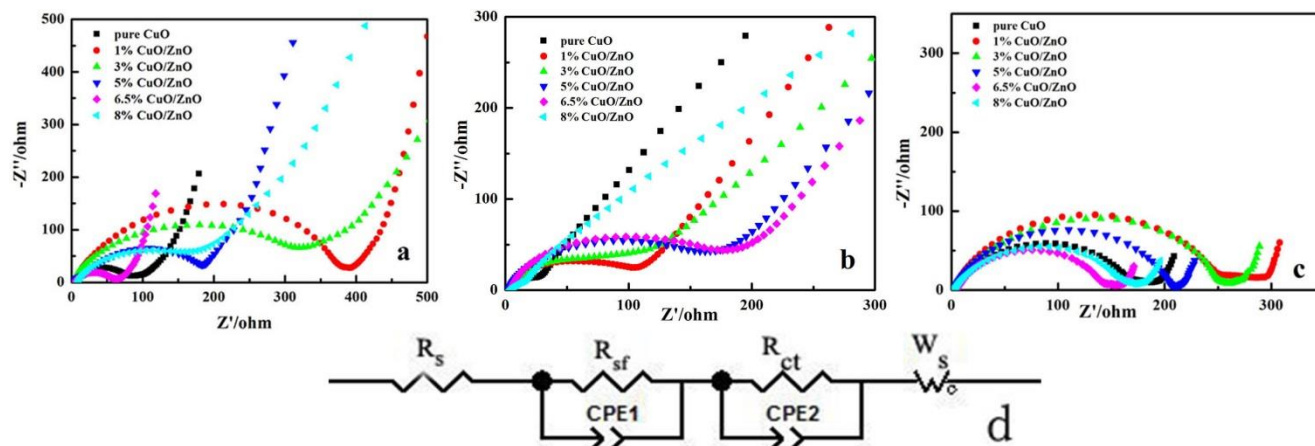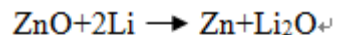
Figure 8. Nyquist plot of Li/CuO@ZnO cells at the open circuit voltage. (a) Nyquist plot after the standing state, (b) Nyquist plot at the end of the charge state after two charge and discharge cycles, (c) Nyquist plot at the end of discharge state after three discharge cycles, (d) Equivalent circuit model for pure CuO and the CuO@ZnO composites

Table 3. Impedance parameters of the samples

Electrode material	Fitting parameters		
	R_s (ohm cm^2)	R_{sf} (ohm cm^2)	R_{ct} (ohm cm^2)
CuO	4.646	9.987	154.8
1% CuO/ZnO	2.613	11.16	240.1
3% CuO/ZnO	3.023	21.98	225.4
5% CuO/ZnO	2.679	6.745	194.4
6.5% CuO/ZnO	4.413	0.8728	137.8
8% CuO/ZnO	2.948	12.53	145.3

Fig. 8 shows the data graphs of CuO and the CuO@ZnO composites with 1%, 3%, 5%, 6.5% and 8% coatings (a) after the standing state, (b) at the end of the charge state after two charge and discharge cycles and (c) at the end of the discharge state after three discharge cycles. It can be seen from the EIS spectrum that the impedance of the CuO material is relatively small after the battery is in the standing state. After coating ZnO, the impedance of the CuO@ZnO composites obviously increased. The semicircular parts for the CuO@ZnO samples with the 1% to 8% coatings are 400 Ω, 310 Ω, 180 Ω, 60 Ω, and 180 Ω, respectively. When the ZnO coating amount was small (1%), the impedance of the CuO@ZnO composites was the largest. As the ZnO coating amount increased, the impedance of the CuO@ZnO composites gradually decreased. When the coating amount was 6.5%, the impedance of the CuO@ZnO composites reached a minimum, and then, the impedance of the CuO@ZnO composites continued to increase with the increasing coating amount. Moreover, the impedance of the CuO@ZnO-6.5% sample reached a minimum, which was less than that of the pure CuO sample. Therefore, the reason for the high stability of the charge and discharge cycling of the CuO@ZnO-6.5% sample in the lithium-ion battery due to its relatively low impedance.

The Nyquist plots of the impedance data were obtained after 2 cycles of constant current charge and discharge (at the end of charging) and 2.5 cycles (at the end of discharge) under the condition of a 0.2 C, as shown in Fig. 8(b) and 8(c). After the cycling, the impedance of all the batteries decreased. With the increasing ZnO coating amount, the impedance of the CuO@ZnO composite material gradually increased. When the coating amount was 6.5%, the impedance of the CuO@ZnO composite material reached its maximum. Later, as the ZnO coating amount increased, the impedance of the CuO@ZnO composite material gradually decreased. At the end of 2.5 cycles of discharge, the impedance change for all materials was the same as the trend observed for the battery after the standing state. The semicircular parts for the CuO@ZnO samples with the 1% to 8% coatings were 300 Ω, 250 Ω, 210 Ω, 150 Ω, and 170 Ω, respectively. However, all materials had a relatively small impedance. The impedance of the CuO@ZnO-6.5% sample was approximately 150 Ω, which was less than the impedance of the pure CuO. Based on the above impedance analysis, it could be concluded that the reason for the higher charging and discharging cycle stability of the CuO@ZnO-6.5% sample was related to the low impedance.

A typical Nyquist plot is composed of a circle in the high-frequency area and a line in the low-frequency region. Further, the intercept on the Z′ represents the ohmic resistance (Rs). Meanwhile, the resistance of SEI film (Rsf) and the charge transfer resistance (Rct)semicircle locate in the high-frequency region . The line stands, Warburg impedance (Ws), is associated with the Li$^+$ diffusion in active material[34]. The EIS results at the end of the discharge state after three discharge cycles were analysed using ZsimpWin software. The equivalent circuit model for the pure CuO and CuO@ZnO composites is shown in Fig. 8d. As expected, the CuO@ZnO-6.5% electrode exhibited much lower Rct and Rs values than the other electrodes.

4. CONCLUSION

CuO@ZnO core-shell composites were successfully prepared by a facile method. After the formation of CuO@ZnO, the cyclic performance as an anode for lithium-ion batteries improved, and

the CuO@ZnO-6.5% sample had a good lithium-ion ability. When evaluated as lithium-ion battery (LIB) anodes, electrochemical testing showed that the CuO@ZnO composite electrode exhibited a high specific capacity of 300 mAh g^{-1} at 0.2 C after 100 cycles, and the CuO@ZnO-6.5% sample exhibited a high specific capacity of 459.5 mAh g^{-1} at 0.2 C after 500 cycles. In this context, a certain amount of ZnO coating provides an effective way to improvethe capacity fading of transition metal oxide materials, and further promote the development of anode materials for LIBS.

References

1. H. liu, L. Shi, D. Li, J. Yu, H.-M. Zhang, S. Ullah, B. Yang, C. Li, C. Zhu, J. Xu, *J. Power. Sources*, 387 (2018) 64.
2. Z. Tu, G. Yang, H. Song, C. Wang, *ACS Appl. Mater. Interfaces*, 9 (2017) 439.
3. N.R. Chodankar, D.P. Dubal, Y. Kwon, D.H. Kim, *Npg Asia Mater.*, 9 (2017) e419.
4. H. Yang, K. Zhang, W. Yang, Y. Chao, S. Lin, *J. Phys. Chem. Solids*, 115 (2018) 317.
5. H. Wang, X. Yang, Q. Wu, Q. Zhang, H. Chen, H. Jing, J. Wang, S.B. Mi, A.L. Rogach, C. Niu, *ACS Nano*, 12 (2018) 09092.
6. K. Wu, D. Liu, T. Yun, *Electrochim. Acta*, 263 (2018) 515.
7. Y. Kim, Y. Noh, H. Han, J. Bae, S. Park, S. Lee, W. Yoon, Y.K. Kim, H. Ahn, M.-H. Ham, *J. Phys. Chem. Solids*, 124 (2019) 266.
8. G. Carbonari, F. Maroni, S. Gabrielli, A. Staffolani, R. Tossici, A. Palmieri, F. Nobili, *ChemElectroChem*, 6 (2019) 1915.
9. P. Huang, M. Zhao, B. Jin, H. Li, Z. Zhu, L. Jiang, Q. Jiang, *Dalton Transactions*, 47 (2018) 14540.
10. S. Zhu, M. Wu, M.-H. Ge, H. Zhang, S.-K. Li, C.-H. Li, *J. Power. Sources*, 306 (2016) 593.
11. W. Zhang, Z. Yin, A. Chun, J. Yoo, G. Diao, Y.S. Kim, Y. Piao, *J. Power. Sources*, 318 (2016) 66.
12. C. Wang, Q. Li, F. Wang, G. Xia, R. Liu, D. Li, N. Li, J.S. Spendelow, G. Wu, *ACS Appl. Mater. Interfaces*, 6 (2014) 1243.
13. J. Guo, L. Ma, X. Zhang, Y. Zhang, L. Tang, *Mater. Lett.*, 118 (2014) 142.
14. H. Huang, Y. Liu, J. Wang, M. Gao, X. Peng, Z. Ye, *Nanoscale*, 5 (2013) 1785.
15. H. Yin, X.-X. Yu, Q.-W. Li, M.-L. Cao, W. Zhang, H. Zhao, M.-Q. Zhu, *J. Alloy. Compd.*, 706 (2017) 97.
16. C. Wang, N. Li, D.Y. Li, F.F. Wang, *Asian J. Chem.*, 27 (2015) 2976.
17. Z. Yin, W. Fan, Y. Ding, J. Li, L. Guan, Q. Zheng, *ACS Sustain. Chem. & Eng.*, 3 (2015) 507.
18. Q. Chen, B. Heng, H. Wang, D. Sun, B. Wang, M. Sun, S. Guan, R. Fu, Y. Tang, *J. Alloy. Compd.*, 641 (2015) 80.
19. J. Hou, H. Zhang, J. Lin, X. Qiu, Z. Tang, *J. Mater. Chem. A*, (2019).
20. Y. Wang, X. Jiang, L. Yang, N. Jia, Y. Ding, *ACS Appl. Mater. Interfaces*, 6 (2014) 1525.
21. L. Feng, Z. Xuan, Y. Bai, H. Zhao, L. Li, Y. Chen, X. Yang, C. Su, J. Guo, X. Chen, *J. Alloy. Compd.*, 600 (2014) 162.
22. M.H. Jung, *J. Colloid Interf. Sci.*, 505 (2017) 631.
23. S. Mohapatra, S.V. Nair, D. Santhanagopalan, A.K. Rai, *Electrochim. Acta*, 206 (2016) 217.
24. H. Fan, H. Yu, Y. Zhang, J. Guo, Z. Wang, H. Wang, X. Hao, N. Zhao, H. Geng, Z. Dai, Q. Yan, J. Xu, *Nano Energy*, 33 (2017) 168.
25. W. Chen, H. Zhang, Z. Ma, B. Yang, Z. Li, *J. Mater. Chem. A*, 3 (2015) 14202.
26. G.H. An, D.Y. Lee, H.J. Ahn, *ACS Appl. Mater. Interfaces*, 9 (2017) 12478.

27. Z. Gao, H. Sun, L. Fu, F. Ye, Y. Zhang, W. Luo, Y. Huang, *Adv. Mater.*, 30 (2018) 1705702.
28. A.K. Rai, L.T. Anh, J. Gim, V. Mathew, J. Kang, B.J. Paul, N.K. Singh, J. Song, J. Kim, *J. Power. Sources*, 244 (2013) 435.
29. C. Chen, S.H. Lee, M. Cho, Y. Lee, *Mater. Lett.*, 140 (2015) 111.
30. J. Yang, Q. Wu, X. Yang, S. He, J. Khan, Y. Meng, X. Zhu, S. Tong, M. Wu, *ACS Appl. Mater. Interfaces*, 9 (2016) 354.
31. L. Yang, L. Ying, Z. Min, Y. Hu, P. Hu, M. Zhu, W. Li, Y. Li, *Mater. Lett.*, 171 (2016) 244.
32. Q. Xie, Y. Ma, X. Wang, D. Zeng, L. Wang, L. Mai, D.L. Peng, *ACS nano*, 10 (2016) 1283.
33. X.H. Huang, X.H. Xia, Y.F. Yuan, F. Zhou, *Electrochim. Acta*, 56 (2011) 4960.
34. C. Jiang, J. Wang, Z. Chen, Z. Yu, Z. Lin, Z. Zou, *Electrochim. Acta*, 245 (2017) 279.